Robotics and Computer Integrated Manufacturing 56 (2019) 287–302

Contents lists available at ScienceDirect

Robotics and Computer Integrated Manufacturing

journal homepage: www.elsevier.com/locate/rcim

Full length Article

A CAD/CAE integration framework for analyzing and designing spatial compliant mechanisms via pseudo-rigid-body methods

P. Bilancia*, G. Berselli, L. Bruzzone, P. Fanghella

Department of Mechanical, Energy, Management and Transportation Engineering, University of Genova, Via All'Opera Pia, 15/A, Genova 16145, Italy

ARTICLE INFO

Keywords:
Spatial compliant mechanisms
Distributed compliance
Pseudo rigid body models
Shape optimization
CAD/CAE integration

ABSTRACT

Compliant Mechanisms (CMs) are currently employed in several engineering applications requiring high precision and reduced number of parts. For a given mechanism topology, CM analysis and synthesis may be developed resorting to the Pseudo–Rigid Body (PRB) method, in which the behavior of flexible members is approximated via a series of rigid links connected by spring-loaded kinematic pairs. From a CM analysis standpoint, the applicability of a generic PRB model requires the determination of the kinematic pairs' location and the stiffness of a set of generalized springs. In parallel, from a design standpoint, a PRB model representing the kinetostatic behavior of a flexible system should allow to compute the flexures' characteristics providing the desired compliance. In light of these considerations, this paper describes a Computer-Aided Design/Engineering (CAD/CAE) framework for the automatic derivation of accurate PRB model parameters, on one hand, and for the shape optimization of complex-shape flexures comprising out-of-plane displacements and distributed compliance. The method leverages on the modelling and simulation capabilities of a parametric CAD (i.e. PTC Creo) seamlessly connected to a CAE tool (i.e. RecurDyn), which provides built-in functions for modelling the motion of flexible members. The method is initially validated on an elementary case study taken from the literature. Then, an industrial case study, which consists of a spatial crank mechanism connected to a fully-compliant four-bar linkage is discussed. At first, an initial sub-optimal design is considered and its PRB representation is automatically determined. Secondly, on the basis of the PRB model, several improved design alternatives are simulated. Finally, the most promising design solution is selected and the dimensions of a flexure with non-trivial shape (i.e. hybrid flexure) is computed. This technique, which combines reliable numerical results to the visual insight of CAD/CAE tools, may be particularly useful for analyzing/designing spatial CMs composed of complex flexure topologies.

1. Introduction

Differently from rigid-body mechanisms, which transfer forces and displacements employing traditional kinematic pairs based on conjugate surfaces, Compliant Mechanisms (CMs) gain at least some of their mobility from the deflection of elastic members [1]. Thanks to the absence (or reduced use) of traditional kinematic pairs, which are based on the relative motion of contacting surfaces, CMs are almost not affected by wear, stick-slip phenomena and backlash, thus requiring minimal maintenance with no need for lubrication. In addition, CMs entail fewer components to achieve the desired mobility, possibly leading to one-piece manufactured solutions. Nonetheless, the analysis and synthesis of CMs is more complex when compared to traditional mechanisms. Also, continuous rotational motions cannot be achieved and CMs' resistance to fatigue must be carefully addressed via either experimental characterization (see, e.g., [2]) or dedicated simulation tools (such as *Ansys*, see, e.g., [3]). Some CMs' application areas include near-constant-force and non-linear springs [4,5], compliant actuators [6], monolithic cardan/spherical joints [7,8], micro-manipulators [9,10] and micro-grippers [11] for precision assembly (see [12] for an interesting review of design alternatives in this application area).

In general, CM design is primarily made difficult by the presence of finite deflections of the flexible members, possibly causing undesired deformations (i.e. *cross-axis* and *parasitic error motions* [13,14]), whose effects are usually more pronounced in case the compliance is distributed along slender beam-like structures. Consequently, the necessity to provide the engineering community with effective tools for CM analysis and synthesis has led to the development of several theoretical and/or numerical methods, which are well summarized in [15]. For instance, the conceptual design of flexure-based CMs has been tackled

* Corresponding author.
E-mail address: pietro.bilancia@edu.unige.it (P. Bilancia).

https://doi.org/10.1016/j.rcim.2018.07.015
Received 13 March 2018; Received in revised form 31 July 2018; Accepted 31 July 2018
Available online 01 September 2018

by means of the *Constraint-Based Design Approach* (CBDA), which is described in e.g. [16]. The CBDA leverages on the evidence that any motion of a rigid body is basically determined by the constraints' position and orientation (i.e. the *constraint topology*). Also, a mathematical formulation of the CBDA, based on the screw theory formalism, has been adressed in [17]. In parallel, the *Freedom And Constraint Topology* (FACT) method, described in [18,19], combines qualitative information about the flexure system's degrees of freedom and its constraint topology, in order to investigate the relationships between all possible flexure designs and related displacements. Then, the shapes of the deformable members, which allow realizing a desired motion of a point of interest, are selected on a map in which all known shape combinations are distributed over the design space. On the other hand, quoting [20], when the FACT method is used for designing multi degree-of-freedom CM, the quantitative modelling of the motion characteristics is not involved. Therefore, FACT-based CM design can be improved by employing the so-called *Position-Space-based Reconfiguration* (PSR) approach, which allows to reconfigure a CM designed for a specific task, with the aim of minimizing its parasitic motions [20–22]. Another alternative method for generating viable initial solutions directly from problem specifications leverages on the concept of *basic compliant building blocks*, which are well described in [23]. However, whenever strict tolerances on the desired displacement are required, a further optimization procedure is necessary after the preliminary study. Further, also topological optimization routines (or, more generally, *continuum structure optimization approaches* [15]) are applicable for the synthesis of distributed compliant devices with complex shape [24]. Nonetheless, a well-known drawback of topology optimization is the possibility to generate design solutions comprising singularities (like punctual flexural structures). At last, more traditional techniques such as the Finite Element Method (FEM) and, where available, analytical solutions, might be very accurate but are far too complicated to be used in either the conceptual design phase or in the industrial scenario, where tools providing ease-of-use and limited computational costs are largely needed.

In this context, a powerful method for CM analysis/synthesis is the Pseudo-Rigid-Body (PRB) approach, which describes a complaint mechanism by a series of rigid links connected through spring-loaded kinematic pairs, such as Spherical (S), Prismatic (P) or Revolute (R) joints (also called *characteristic pivots*). Once a PRB topology has been selected (namely, number and type of kinematic pairs), specific optimization routines, such as gradient-based [25] or non-gradient based methods [26], are employed in order to assess the values of both springs' stiffness and pivots' location allowing a PRB-based mechanism to replicate the CM kinetostatic behavior as close as possible. For example, Fig. 1a depicts a *planar parallel guide CM* [27], namely a device largely employed in e.g. micro-motion stages [28] composed of a pair of *fixed-guided flexible beams* [29]. In parallel, Fig. 1b shows a possible PRB topology of such device, where each beam is modelled via two spring-loaded R joints. In this particular case, for given loads and boundary conditions, the pivots' location and stiffness have been determined so as to minimize the difference in the trajectory of body c (platform) in the two cases (i.e. actual CM and related PRB model). In general, it may happen that the chosen PRB representation does not capture the deformations of the compliant elements up to a level of accuracy that is deemed sufficient for the application at hand, thus forcing the designer to increase the PRB model's degrees of freedom. An example of such topology modification is depicted in Fig. 1c, where each flexible member is now represented via a spring-loaded 3R chain (as suggested in [30]). In practice, PRB techniques basically offer two advantages: *i*) enhanced computational efficiency during CM simulation if compared to the FEM approach; *ii*) possibility to employ well established methods and software tools, such as common multibody (MBD) environments, specifically conceived for analyzing rigid-link mechanisms. On the other hand, PRB limitations, whose acceptability has to be evaluated on a case by case basis, may be listed as follows: *i*) possibility for the PRB parameters to become load dependent in case of insufficient mobility of the chosen PRB topology (refer to [31] for an overview and a comparison of several PRB topologies); *ii*) incapability to capture non-linear effects arising during large deflections, such as material non-linearity, geometric non-linearity and load-stiffening effects [13,15]. Henceforth, CM architectures computed via the PRB method are usually validated by means of FEM or experiments at the end of any design process. Despite these limitations, PRB techniques have been successfully used for identifying bi-stability [32], for evaluating CM workspaces [33], for comparing compliant joints morphologies [34], and for model-based control of compliant mechatronic devices [35].

Owing to this brief state-of-the-art overview, an assessment of the previous researches highlights the following issues:

- The determination of the optimal PRB parameters starts from the knowledge of the load-deflection characteristics of the CM under investigation, which is usually derived resorting to 2D or 3D analytical models (e.g. straight beams with rectangular/circular cross section or notch hinges [36–38]). This approach, based on closed form solutions, is accurate and very useful when choosing and benchmarking a suitable PRB topology. Nonetheless, purely analytical methods fail to provide useful information when designing generic flexure geometries (see e.g. the so-called *hybrid flexures* [39]), whose use may be beneficial for optimizing the mechanism selective compliant behavior [34].
- Although some very interesting theoretical works concerning PRB approaches for spatial CMs have recently appeared [40,41], the majority of applications presented the past literature takes into account CMs subjected to planar motions only, a possible reason being the complexity of analytical methods when dealing with spatial deformations;
- In terms of computer-aided design of mechanisms, there has been a number of numerical solvers developed throughout the years (see [42] for a review), comprising nonlinear FEM and MBD packages. Nonetheless, practical methods, which take advantage of the capabilities of integrated Computer-Aided-Engineering (CAE)

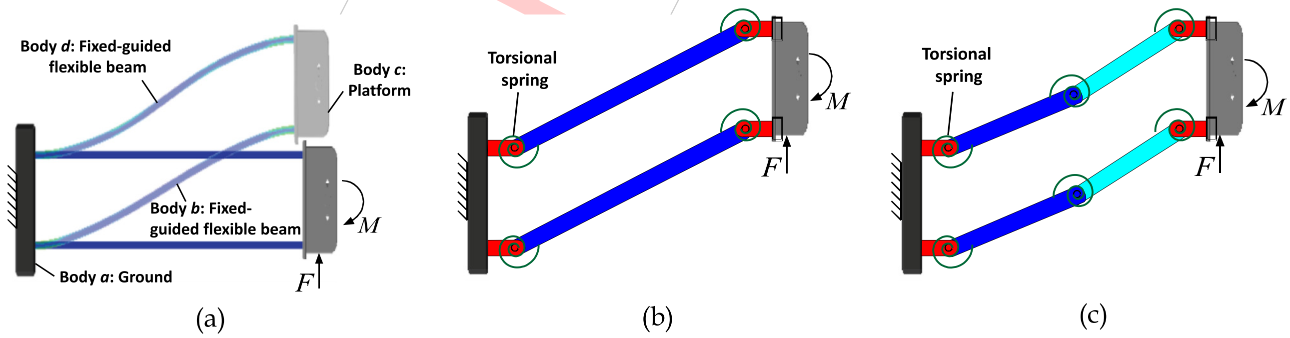

Fig. 1. Example of a parallel guide CM (a) and related 2R (b) and 3R (c) PRB representation.

environments, when specifically applied for CM analysis/design, have been scarcely described and should be further investigated.

As for the latter point, for what concerns specific CM design tools, a first example is represented by *SPACAR* [43], an open-source code that can simulate the motion of 3D flexible devices. More recently, a *Matlab*-based, object-oriented software tool called *DAS-2D* [42] has been released for the same purpose. Possible drawbacks of the abovementioned tools are the rather basic graphic interface and the use of 1D beam elements for structural analysis. Therefore, by using either *SPACAR* or DAS-2D, it is currently impossible to manage compliant members with non-conventional shape, whose use could be beneficial in many applications. In addition, DAS-2D is limited to planar case studies, although a 3D version (i.e. DAS-3D) is announced in development. At last, for what concerns general-purpose commercial CAE tools, some MBD tools, such as *RecurDyn*, can be used for the virtual prototyping of flexible multibody systems in the large deflection range. Even so, in case the shape of the compliant members needs to be optimized on the basis of a user-defined cost function, the designer may rapidly face the intrinsic limits of all the above mentioned packages. In practice, nowadays, a CAD/CAE-based environment easily allowing for CM shape optimization is non-existent. Therefore, similarly to [44], the only viable strategy seems to be the integration of multiple platforms, namely a parametric CAD for shape modelling, a CAE solver for model solution and an external optimizer

Owing to these considerations, the purpose of this paper is to describe and test a novel CAD/CAE framework specifically conceived for analyzing and designing spatial CMs by means of the PRB method. Such framework allows for data exchange between a parametric CAD (*PTC CREO*), the abovementioned CAE software *RecurDyn*, and a set of optimization routines written in *Matlab*. In particular, a clear advantage in employing a parametric CAD/CAE is the possibility for the user to capture *design intents* using features and constraints [45], thus allowing to automate repetitive changes while maintaining a complete freedom in the creation of complex 3D geometries suitable to a large variety of design goals. Moreover, by this general approach, not only geometries but also material properties can be parameterized: for instance, the material Young's modulus may be function of some flexure geometrical parameters, thus implementing the suggestions very recently highlighted in [46], which propose the use of an equivalent modulus, whose value is dependent on the flexure out-of-place thickness, whenever idealized elements or models are employed (such as “beam” elements or planar stress / planar strain hypotheses). Building upon these promising features, the effectiveness of the proposed tool will be tested on a simple case study taken from the literature [1], namely a fixed-guided flexible beam as the one depicted in Fig. 1a. Then, a more complex case will be considered, in order to test the tool accuracy when dealing with 3D motions and deformable parts with complex geometry. The compliant system under investigation consists of a spatial slider-crank mechanism connected to a compliant four-bar linkage subjected to out-of-plane loads. The resulting PRB model, which closely replicates the initial (sub-optimal) design, comprises four Spherical (S) joints with three-dimensional rotational springs mounted in parallel. After the numerical testing of several design alternatives and the selection of the most promising solution, the final CM design (composed of two hybrid flexures) is derived, confirming the practical usability of the proposed multi-software framework. In all these cases, the material properties will be assumed as constant.

The rest of the paper is organized as follows: Section 2 outlines a series of possible CM designs steps, leveraging on the capabilities offered by the mentioned software framework; Section 3 describes how a *fixed-guided flexible beam* (see Fig. 1a) may be analyzed and designed by means of theoretical methods and furtherly highlights the complexity of the analytical approach in case of out-of-plane loads; Section 4 reports the in-depth description of the overall CAD/CAE tool, which is actually conceived to overcome the limitations of the theoretical approaches; Sections 5 and 6 reports about the method validation and its implementation on the described spatial CM; Section 7 provides the concluding remarks.

2. Overview of the proposed CM analysis and design approach

A conceptual schematic of possible steps leading to the optimal design of a spatial, distributed CM with complex-shape flexures is depicted in Fig. 2.

Such steps can be described as follows:

- *#Step 1*: starting from an initial, sub-optimal, design solution where the CM topology is defined, an automatic routine provides a PRB representation of the system. In the following, this step will be referred to as *PRB Derivation Process*;
- *#Step 2:* on the basis of a PRB model, several design alternatives can be tested by simulation, the only limit being that the initial mechanism topology shall be maintained. Naturally, the PRB representation allows to simulate each design variant in a very quick and efficient way (i.e., the computational time is reduced of two order of magnitude as compared to simulations based on FEM [47]);
- *#Step 3*: once the most promising solution (still based on a PRB representation) is found, the final shape of the flexible members is determined by leveraging on the abovementioned CAD/CAE

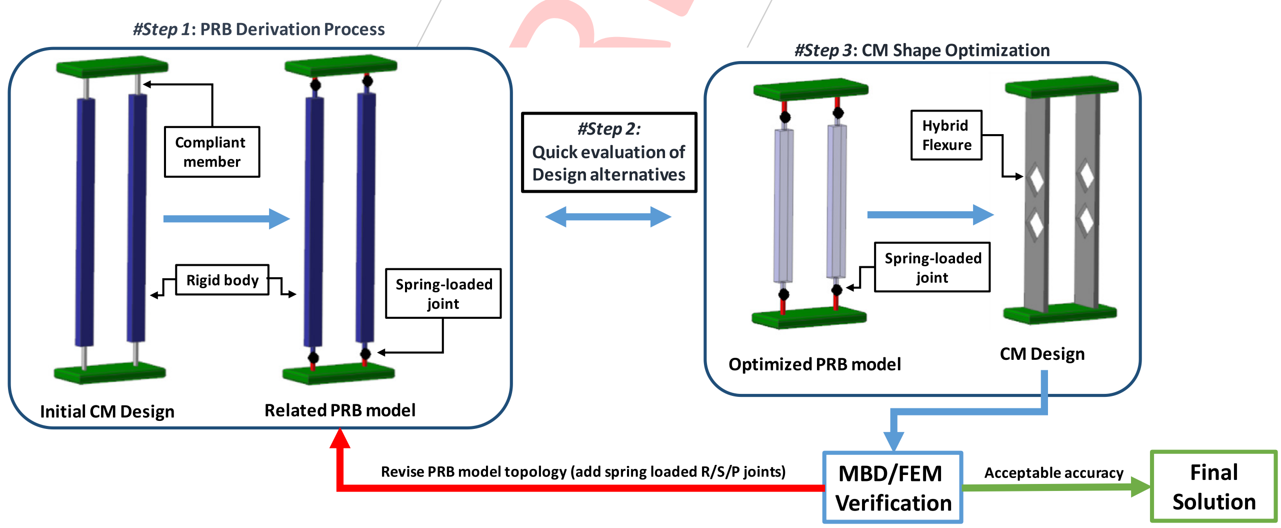

Fig. 2. CM Design method leveraging on the PRB technique.

integration routines. Note that the final CM design fully replicates the behavior of its PRB counterpart. In addition, also flexures with complex shape (i.e. hybrid flexures) can be designed. In the following, this last step will be referred to as *CM Shape Optimization.*

At last, when a suitable CM design has been produced, the initial assumption about the PRB topology are verified against numerical data coming from MBD/FEM simulations. If the obtained accuracy is envisaged as sufficient for the considered application, the obtained hybrid flexure geometries represents the final solution. In any other case, a design iteration will be necessary, based on an increment of the number of degrees of freedom as compared to the initial PRB model.

3. Analysis and design of fixed-guided beams via analytical methods

This section recalls the modelling of the *fixed-guided flexible segment* (see Fig. 1a), thus providing both the necessary analytical background to derive a PRB model and the means to compute the dimensions of a flexure with simple shape on the basis of the desired stiffness characteristics. The schematic layout and the boundary conditions of such slender beam flexure are depicted in Fig. 3a, the related 2R PRB model is shown in Fig. 3b, the free-body diagram of one half of the beam and its 1R PRB model are reported in Figs. 3c and 3d. In particular, one end of the flexure is clamped to the ground, whereas the other end is guided to maintain absence of rotation. In order to obtain this configuration, a resultant clockwise moment M must be applied at the beam end points, in addition to the vertical force F. Summing moments at either end of the free-body diagram in Fig. 3c yields to the following relations:

$$Fa_c - M = \frac{Fa_c}{2} \rightarrow M = \frac{Fa_c}{2} \tag{1}$$

where a_c is the horizontal distance between beam free and fixed ends (see Fig. 3a). The resulting deflected shape is antisymmetric at its centerline (as shown in Fig. 3a), the angular deflection of the beam, ϑ, reaching its maximum for $\vartheta_{y=a_c/2} = \vartheta_0$ where the curvature is zero. Being directly related to the beam curvature, the moment at $y = a_c/2$ is null.

Consequently, in order to evaluate the beam tip deflection when subjected to force F and moment M, due to symmetry, a single half-beam subjected to the only vertical force F can be considered. Subsequently, the results obtained by means of the large deflection beam theory (elliptic integral approach [1]) must be multiplied by a factor of two, as follows:

$$\alpha_t = \frac{2}{\sqrt{2}} \int_0^{\vartheta_0} \frac{d\vartheta}{\sqrt{\sin\vartheta_0 - \sin\vartheta}} \tag{2}$$

$$\frac{a_c}{l} = \frac{2}{\alpha_t\sqrt{2}} \int_0^{\vartheta_0} \frac{\cos\vartheta\, d\vartheta}{\sqrt{\sin\vartheta_0 - \sin\vartheta}} \tag{3}$$

$$\frac{b_c}{l} = \frac{2}{\alpha_t\sqrt{2}} \int_0^{\vartheta_0} \frac{\sin\vartheta\, d\vartheta}{\sqrt{\sin\vartheta_0 - \sin\vartheta}} \tag{4}$$

where l is the beam length, a_c/l and b_c/l are, respectively, the normalized horizontal and vertical displacement of the tip, and α_t is the *non-dimensional transverse load index* [1], defined as:

$$\alpha_t = \sqrt{\frac{Fl^2}{EJ_{zz}}} \tag{5}$$

where E is the Young modulus of the beam material and J_{zz} is the moment of inertia of the beam cross section along an axis (z-direction) perpendicular to the motion plane. In this particular situation, a 2R-PRB

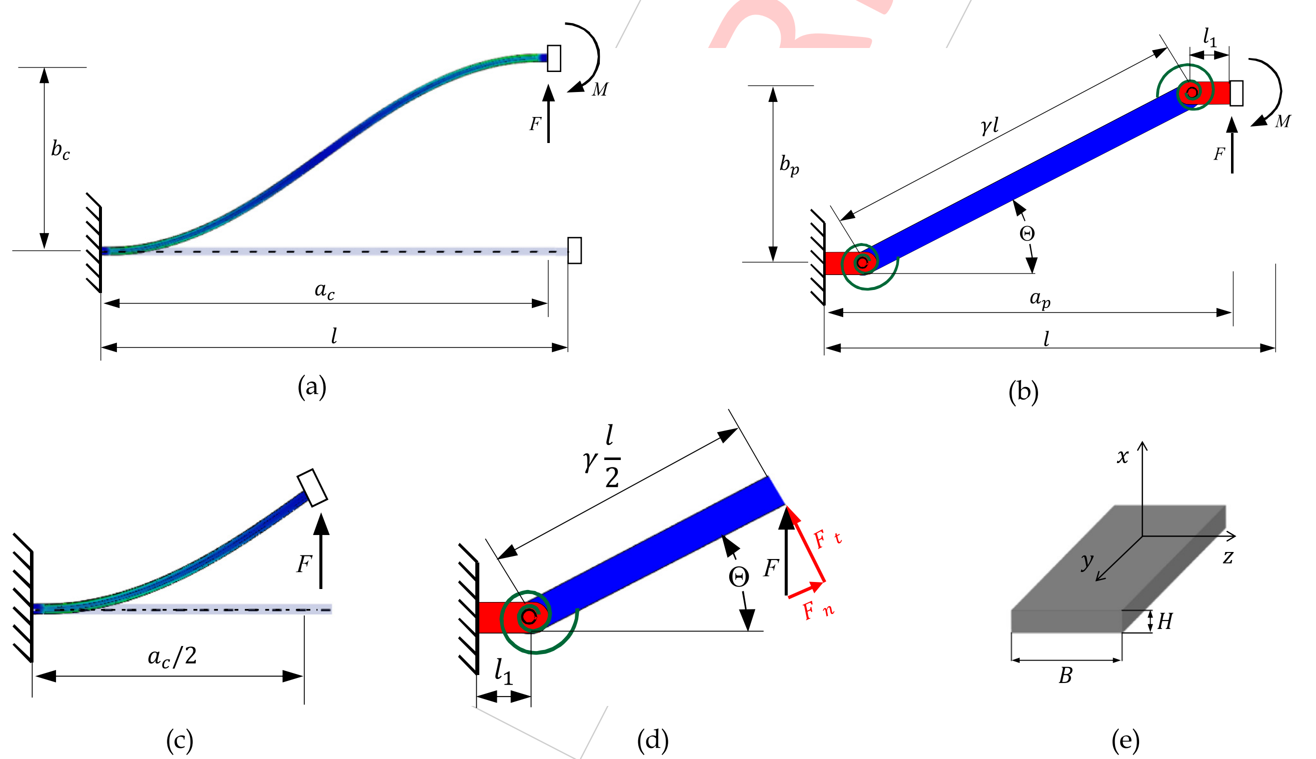

Fig. 3. (a) fixed-guided flexible beam (undeflected + deflected configurations); (b) related 2R PRB; (c) half-beam schematic subjected to end force; (d) half-beam PRB model; (e) Beam cross section.

model, consisting of three rigid links connected by two symmetrically-disposed revolute pairs, is shown in Fig. 3b. Furthermore, two torsional springs with same stiffness are located over the revolute joints in order to approximate the beam compliance. Therefore, such 2R-PRB model requires two characteristic parameters to describe the kinematic and the force-deflection behavior of the related CM. By employing the same notations suggested in [1], the PRB parameters are indeed the *characteristic radius factor* (γ) and the *stiffness coefficient* (K_Θ). Within the PRB approximation, the length of the links (i.e. $l_1 = l_3$ and l_2, see Fig. 3b) and, consequently, the horizontal, a_p, and vertical, b_p, positions of the PRB model's end point can be defined as function of γ. The following relations hold:

$$l_1 = l_3 = \frac{(1-\gamma)l}{2};\;\; l_2 = \gamma l; \tag{6}$$

$$a_p = l(1-\gamma(1-\cos(\Theta)));\;\; b_p = \gamma l\sin(\Theta); \tag{7}$$

In parallel, the stiffness of the torsional springs can be expressed considering the half-beam and the related PRB model (see Fig. 3d). The PRB angle Θ is proportional (with K constant) to the torque at the revolute joint, given by $T = F_t\frac{\gamma l}{2}$.

Combining the equations, the force can be expressed as follows:

$$F_t = \frac{2K\Theta}{\gamma l} \tag{8}$$

where F_t is the transverse component of the vertical force F. Moreover, considering also the parameter α_t, the force-deflection relationships may be written as:

$$\alpha_t^2 = \frac{F_t l^2}{EJ_{zz}} = K_\Theta\Theta \tag{9}$$

where K_Θ is, as previously introduced, the stiffness coefficient. Then, by means of Eqs. (8) and (9), the constant spring stiffness of each revolute joint of the half-PRB model can be formulated as:

$$K = \gamma K_\Theta\frac{EJ_{zz}}{2l} \tag{10}$$

Eq. (10) has to be adapted in order to comply with the complete PRB model, that involves two revolute pairs and a total length equal to l. In this case, Eq. (9) becomes $\alpha_t^2 = 2K_\Theta\Theta$, the final stiffness value being given by:

$$K = 2\gamma K_\Theta\frac{EJ_{zz}}{l} = \tau\frac{EJ_{zz}}{l} \tag{11}$$

where $\tau = 2\gamma K_\Theta$. The numerical values of γ and K_Θ and, as a consequence, of τ can be assessed via optimization techniques aiming at providing PRB models which can optimally replicate the trajectory of the beam free end during deformation, expressed by Eqs. (2)–(4). In particular, the numerical problem is divided in two different steps. The first step allows to determinate the value of γ, so that the PRB linkage end-point's trajectory replicates (with an acceptable error) the CM's deflection path, at least up to a user-defined maximum angle, Θ_{max}, having defined the so-called *PRB angle*, Θ, as follows:

$$\Theta = atan\left(\frac{b_p}{a_p - l(1-\gamma)}\right) \tag{12}$$

Recalling from [1], the optimization problem may be formalized as finding the value of γ which maximizes the PRB angle Θ (from Eq. (12)), which is subject to the parametric constraint

$$e_{tra}(\Theta) = \frac{\sqrt{\left(\frac{a_c}{l} - \frac{a_p}{l}\right)^2 + \left(\frac{b_c}{l} - \frac{b_p}{l}\right)^2}}{\sqrt{\left(1 - \frac{a_p}{l}\right)^2 + \left(\frac{b_p}{l}\right)^2}} \le (e_{tra})_{max}\text{ for } 0 < \Theta < \Theta_{max} \tag{13}$$

where $e_{tra}(\Theta)$ is the relative deflection error and a_c, b_c, a_p, b_p are respectively defined in Eqs. (3),(4) and (7). Once the value of γ has been obtained, the second step considers the rotational springs placed in parallel to the R joints, with the aim of finding the optimal K_Θ value, so that the PRB model mimics the CM force-displacements behavior within the range $0 < \Theta < \Theta_{max}$. Recalling the design process depicted in Fig. 2, the abovementioned procedure basically covers the first design step (i.e. the PRB derivation process).

On the other hand, for what concerns the actual determination of the flexure geometric parameters starting from a PRB model (i.e. the third step in Fig. 2) some additional assumptions are needed, namely cross section type and flexure material properties. Let one then consider a slender beam with rectangular cross section as depicted in Fig. 3e. The moment of inertia of the beam cross section is:

$$J_{zz} = \frac{BH^3}{12} \tag{14}$$

As previously said, it is also necessary to consider the maximum stress associated to the load condition. Considering bending as the predominant loading mode, the associated stress is given by:

$$\sigma_{max} = \frac{M_{max}}{W} = \frac{6M_{max}}{BH^2} \tag{15}$$

where W is the cross section's modulus, whereas B and H are, respectively, the cross section's width and thickness. Since the maximum bending moment $|M_{max}|$ is placed, for this configuration, at each beam end, Eq. (15) evolves in:

$$\sigma_{max} = \frac{3Fa_c}{BH^2} \tag{16}$$

In order to avoid failures, the maximum stress σ_{max} shall be always lower than the material yield strength, σ_s. In conclusion, the cross section width, B, and thickness, H, can be determined by solving a system of equations, in which the reference PRB model is completely defined, so that the Θ angle is known. The first system includes Eqs. (11) and (14):

$$\begin{cases} K = \tau\frac{EJ_{zz}}{l} \\ J_{zz} = \frac{BH^3}{12} \end{cases} \rightarrow BH^3 = \frac{12Kl}{E\tau} \tag{17}$$

The final system also considers Eq. (16), having selected a maximum stress σ_{max} and having imposed $a_p = a_c$ (namely, the compliant system to be designed replicates the reference PRB model). The cross section dimensions are finally determined as follows:

$$\begin{cases} BH^3 = \frac{12Kl}{E\tau} \\ \sigma_{max} = \frac{3Fa_p}{BH^2} \end{cases} \rightarrow \begin{cases} H = \frac{4Kl\sigma_{max}}{E\tau Fa_p} \\ B = \frac{3Fa_p}{\sigma_{max}H^2} \end{cases} \tag{18}$$

Note that the abovementioned theoretical procedure is quite straightforward, although based on simplifying assumptions (e.g. bending stress only) and only applicable to the design of slender beam-like segments with uniform cross section subjected to planar deformations only.

For what concerns flexures subjected to out-of-plane deformations (i.e. spatial motions), the derivation of a suitable PRB model, along with the flexure sizing starting from a PRB model (i.e. respectively the first and third steps in Fig. 2), the abovementioned theoretical procedure is rather complex [41], so that a numerical approach seems preferable.

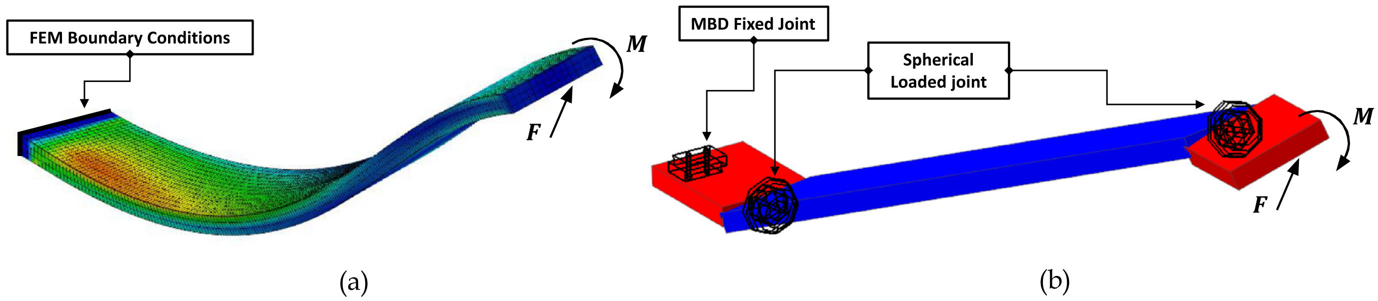

Fig. 4. (a) Cantilever flexible beam subjected to out-of-plane loads; (b) related 2S PRB.

Let one then consider, once again, a slender flexible beam subjected to out-of-plane loads (as shown in Fig. 4a). In this particular situation, a 2S-PRB model, consisting of three links connected by two spring-loaded S pairs, is shown in Fig. 4b.

Considering the rectangular cross section depicted in Fig. 3e, along with a reference frame in which the principal beam axis is directed in the *y*-direction, the *x*-axis and the *z*-axis respectively defining the direction of the higher (*primary*) and smaller (*secondary*) beam cross-section moments of inertia (also shown Fig. 3e), the values for the PRB rotational stiffness can be formulated as follows [40,48]:

$$\begin{cases} K_{\vartheta x} = \mu \frac{EJ_{xx}}{l} = \mu \frac{EHB^3}{12l} \\ K_{\vartheta y} = \varepsilon \frac{2G(J_{xx}+J_{zz})}{l} = \varepsilon \frac{2GBH(B^2+H^2)}{12l} = K_{\vartheta x}\frac{\varepsilon}{\mu}\frac{2G(B^2+H^2)}{EB^2} \\ K_{\vartheta z} = \tau \frac{EJ_{zz}}{l} = \tau \frac{EBH^3}{12l} = K_{\vartheta x}\frac{\tau}{\mu}\frac{H^2}{B^2} \end{cases} \tag{19}$$

where $K_{\vartheta x}$, $K_{\vartheta y}$ and $K_{\vartheta z}$ are, respectively, the stiffness related to the rotations around the *x, y*, and *z* axis, J_{xx} is the moment of inertia of the beam cross section along *x* axis, *G* is the shear modulus of the material and μ, ε and τ are specific constants. In practice, in case of planar CMs, the PRB model derivation process requires the determination of the R joints location and a single stiffness coefficient, $K_{\vartheta z} = K$, for each rotational pair (or, in turn, the values of γ and τ, see Eqs. (6) and (11)). On the other hand, when dealing with spatial CMs and spring-loaded S joints, two additional rotational stiffness, namely $K_{\vartheta x}$ and $K_{\vartheta y}$ shall be determined (or, in turn, the values of μ and ε, see Eq. 19). In such case, the numerical optimization procedure presented hereafter can provide reliable results in an efficient manner.

4. Description of the CAE-based procedure

As previously recalled, for a given CM topology, the determination of the PRB parameters can be achieved by means of a variety of techniques (see, e.g., [26,31]). On the other hand, for what concerns the determination of a hybrid flexure geometry mimicking a reference PRB model, no general analytic solution is available. In this case, the problem can be tackled resorting to a software tool enabling an effective search of a CM optimal design starting from a parametric CAD/CAE model. Essentially, such tool aims at solving a design optimization problem, having defined an objective function (alternatively called performance index), lower and upper bounds for a set of parameters representing design variables in the CAE environment, and a set of constraints. As regards the CM design by means of the PRB method, once the PRB topology is defined, external loads (or displacements) are applied to both a CM model (comprising deformable links) and a PRB system (comprising only rigid links and lumped springs). On one hand, the CM can be analyzed by means of nonlinear FEM or, if possible, via theoretical methods (such as the Euler-Bernoulli beam theory). On the other hand, the PRB system can be analyzed resorting to the free-body diagram approach, to the principle of virtual works [1], or by means of MBD tools. The definition of the objective function is then obtained by a norm of the distance of the trajectories of one reference frame of interest measured on both flexible CM model and PRB-based mechanism. The optimization problem, whose objective function will be hereafter referred to as *trajectory error*, e_{tra}, can be formulated as follows:

$$\textbf{Minimize}\ e_{tra}(p_1,\cdots,p_n) = \sqrt{\frac{1}{Q}\sum_{i=1}^{Q}\left[\sum_{j=1}^{3}\frac{|x_j^C - x_j^P|}{l} + \sum_{k=1}^{3}|\theta_k^C - \theta_k^P|\right]^2} \tag{20}$$

$$\textbf{Subjectto} \begin{cases} p_{1,\min} \le p_1 \le p_{1,\max} \\ \vdots \\ p_{n,\min} \le p_n \le p_{n,\max} \\ f(p_1,\cdots,p_n) = p_{n+1},\cdots,p_{n+m} \end{cases} \tag{21}$$

where *n* is the number of design parameters (denoted as *p*), x_j^C, x_j^P, θ_k^C, θ_k^P are, respectively, translations and rotations (defined, for instance, via the Euler angles convention) of the chosen reference frame fixed to both one link of the CM (superscript *C*) and of the PRB (superscript *P*), and *l* is the flexure length (as in Fig. 3a). The performance index e_{tra} is then evaluated through a series of *Q* simulation steps. Eq. (21) formalizes the optimization constraints in terms of lower and upper bounds of the design parameters (inequality constraints) and/or (nonlinear) constraint relations between the design parameters p_1, …,p_n and user-defined constants, p_{n+1},…, p_{n+m}. The performance index represents the root mean square value of the trajectory error computed in *Q* equilibrium mechanism configurations, from the undeformed configuration to the maximum imposed deflection.

An efficient method to determine the relation between the design parameters and the objective function, widely employed in modern design optimization approaches, is based on the use of *meta-models* [49,50], namely suitable approximations of the real objective function, whose construction is based on two essential steps: *Design Of Experiments* (DOE), where the design space is sampled in a discrete number of points, and *Response Surface Modeling* (RSM), which refers to all those techniques employed to create an interpolating or approximating *n*-dimensional hypersurface in the $(n+1)$-dimensional space given by the *n* design variables plus the objective function. The benefit of this approach is that, once the meta-model has been obtained, very quick optimization techniques can be used to determine the stationary points on the response surface. In practice, meta-modeling techniques become useful when it is impossible or too complex to define analytically the correlation between the objective function and the design parameters. Considering the objective function, e_{tra}, and the parameters defined in Eqs. (20) and (21), the selected DOE + RSM procedure provides an approximation, $\hat{e}_{tra}$, of the actual function, e_{tra}, which may be formulated as follows:

$$\boldsymbol{X} = [p_1, \ldots, p_n] \tag{22}$$

$$\boldsymbol{Y} = e_{tra}(\boldsymbol{X}) = \hat{e}_{tra}(\boldsymbol{X}) + \varepsilon(\boldsymbol{X}) \rightarrow \widehat{\boldsymbol{Y}} = \hat{e}_{tra}(\boldsymbol{X}) \tag{23}$$

where $\widehat{\boldsymbol{Y}}$ is the is the estimated approximate response function and $\varepsilon(\boldsymbol{X})$ is the error related to the meta-modelling step. Further insight of this numerical procedure can be found in [51].

4.1. Automatic derivation of PRB model parameters via CAE tools

Concerning the PRB derivation procedure (*#Step 1* in Fig. 2) and assuming that a set of n_s spring-loaded spherical pairs are employed in the PRB representation of a generic spatial CM, the minimization problem previously introduced in Eqs. (20) and (21) is used in order to determine both springs' location and generalized rotational stiffness. Therefore, recalling that such PRB system can be fully described by $n-1$ parameters γ (defining the kinematic pair location via Eq. (6)), along with a set of three parameters μ, ε, τ for each spring (defining generalized stiffness via Eq. (19)), the DOE + RSM procedure aims at providing the function $\hat{e}_{tra}(\gamma_1, \cdots, \gamma_{n-1}, \mu_1, \cdots, \mu_n, \varepsilon_1, \cdots, \varepsilon_n, \tau_1, \cdots, \tau_n)$, to be subsequently minimized. Such optimization procedure has been previously managed by the authors in [52], where the *RecurDyn*'s internal optimization toolkit (named "*Autodesign*") has been employed and its intrinsic limitations (in terms of meta-modelling capabilities) have been discussed. Extending the abovementioned previous work, in the following, a framework has been developed in which *Matlab* manages the optimization process, along with all the simulations and the data exchange activities. With reference to Fig. 5, for what concerns the PRB derivation of a generic spatial CM with given topology, the procedure involves:

- ***Matlab***, the well-known numerical environment, as MAIN (i.e. governing iteration execution, collecting post-processing data, providing the DOE + RSM phase);
- ***RecurDyn***, a Multi-Flexible Body Dynamics (MFBD) software, as CALCULATOR, to execute PRB simulation and then to compute the objective function at each iteration.

The optimization process is overseen by *Matlab* and leverages on *RecurDyn*'s interfacing capabilities, which allows the use of batch simulation execution: *RecurDyn*'s solver can be run in batch mode through a set of command files, consequently, set up by *Matlab*. The following file types are employed:

- **Scenario File** (.rss file), that contains information about the simulation that has to be performed, such as Simulation Type and Number of Simulation Steps;
- **RecurDyn Design Parameter Files** (.rdp and .rpv files), which contains all the parametric data to be set in the model. In particular, the numerical value of each parameter are stored into such files, that can be created and modified via a *Matlab* function.

In this application, as said, the *trajectory error* defined in Eq. (20) shall be evaluated. Once external loads and/or displacements are defined, the CM behavior is simulated within the MBD tool in order to compute a set of values for x_m^C and θ_n^C. These values are then fed into the PRB model (built within the *RecurDyn* environment), which is used for objective function evaluation. It is important to remark that CM boundary conditions are applied also to the PRB model. For each PRB model solution, representing the K-th iteration of the optimization process, the *trajectory error* is computed on the basis of the values for x_m^C, θ_n^C, x_m^P, θ_n^P. The results obtained for each PRB model simulation

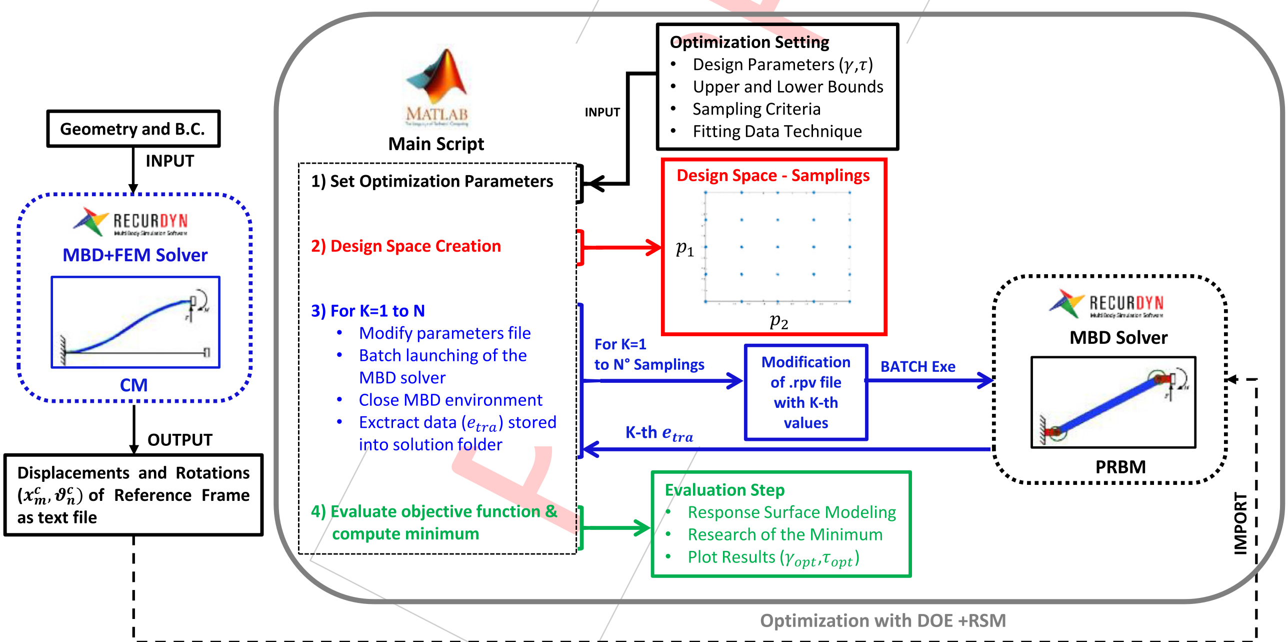

Fig. 5. Schematic of #Step 1 (PRB derivation) optimization loop.

(*trajectory error* versus system configuration) are then exported and stored. In order to manage and solve the optimization problem, the following operations are performed through a sequence of *Matlab* functions:

- **Creation of the Design Space**, based on upper and lower bounds specified for each parameter;
- **Definition of the Sampling Points** over the design space, on the basis of the settings (in terms of sampling criteria and number of samples), defined in the previous step;
- **For** K = 1 **to** Number of Sampling Points
  - **Update** the *RecurDyn* Design Parameter file with the K-th set of values;
  - **Batch *RecurDyn* Execution**;
  - **Extraction** of the K-th results set and evaluation of the objective function $e_{tra}(p_1, ..., p_n)$;

  end
- **Data fitting**, in order to obtain the Response Surface and complete the Meta-Modelling phase;
- **Search of the minimum** via a minimization algorithm.

In this paper, the Full-Factorial criterion and the Radial-Basis-Function (Multi-Quadratic) technique are respectively adopted for the DOE + RSM phase [53]. Subsequently, a deterministic algorithm within *Matlab* is used for finding the minimum of the Response Surface. Since the definition of an initial value (from which the algorithm starts the optimum search) is usually required, in order to avoid local minima, several initial values are tested. Those values are selected among the discrete minima found during the DOE step, as suggested in [51]. A conceptual schematic of the complete optimization process is shown in Fig. 5.

4.2. CAD/CAE-based shape optimization of compliant members

As depicted in Fig. 2, after an optimal PRB-based design has been determined, the last design step (i.e. CM Shape Optimization) is used to determine the shape of generic hybrid flexure geometries that can provide the required stiffness. This numerical approach allows to overcome the limitation of several theoretical models, such as the one recalled in Eq. (18) concerning beams with rectangular cross-section only. Consequently, the minimization problem, previously introduced with Eqs. (20) and (21), is again formulated considering as design variables the dimension parameters of the compliant members, so that the design parameters, p_1, ..., p_n, now represent a user-defined set of flexure geometric dimensions set-up within a parametric CAD. Again, the DOE + RSM procedure aims at providing the function $\hat{e}_{tra}(p_1, ..., p_n)$, to be subsequently minimized. Differently from the PRB derivation process, in which parametrization and calculations can be performed by leveraging only on *Matlab* functions managing the MBD environment, in case of CM shape optimization two additional tools are needed. This is due to the necessity to vary the flexure parametric dimensions at each iteration, to regenerate the actual 3D shapes of the flexible links and, consequently, to re-mesh them, to re-set their boundary conditions (connections with other bodies of the system) and to specify material properties. Automatic execution of re-meshing and boundary condition definition are not natively provided by *RecurDyn*, but it is possible to implement them by leveraging on *ProcessNet*, a macro development toolkit integrated within *RecurDyn* and based on C# programming language. A *ProcessNet* script, executing re-meshing, boundary conditions re-settings and material properties definition, can be automatically run when *RecurDyn* is launched in batch modality. Therefore, the *Matlab*-guided framework described in the previous section can be adapted to provide shape optimization capabilities. In this case, the procedure involves:

- ***Matlab*** as MAIN;
- ***RecurDyn*** as CALCULATOR;
- ***PTC Creo*** as Parametric CAD to regenerate 3D shapes;

Similarly, to the schematic reported in Fig. 5, the shape optimization process starts from *Matlab*. As mentioned, the need to change the flexure geometry at every iteration involves the use of a parametric CAD that can be controlled by using a text file, in which geometrical features and dimension parameters are defined. Such text file is modified by *Matlab* and overwritten for every K-th sampling of the design space. In particular, new geometries are generated, exported and then, a specific *ProcessNet* script updates the *RecurDyn* model with the K-th CAD file. The structure of the *ProcessNet* script considered in this paper is represented in Fig. 6, which provides an overview of the main sections of the code. For a detailed explanation of each command/action, the interested reader may refer to the *ProcessNet* manual.

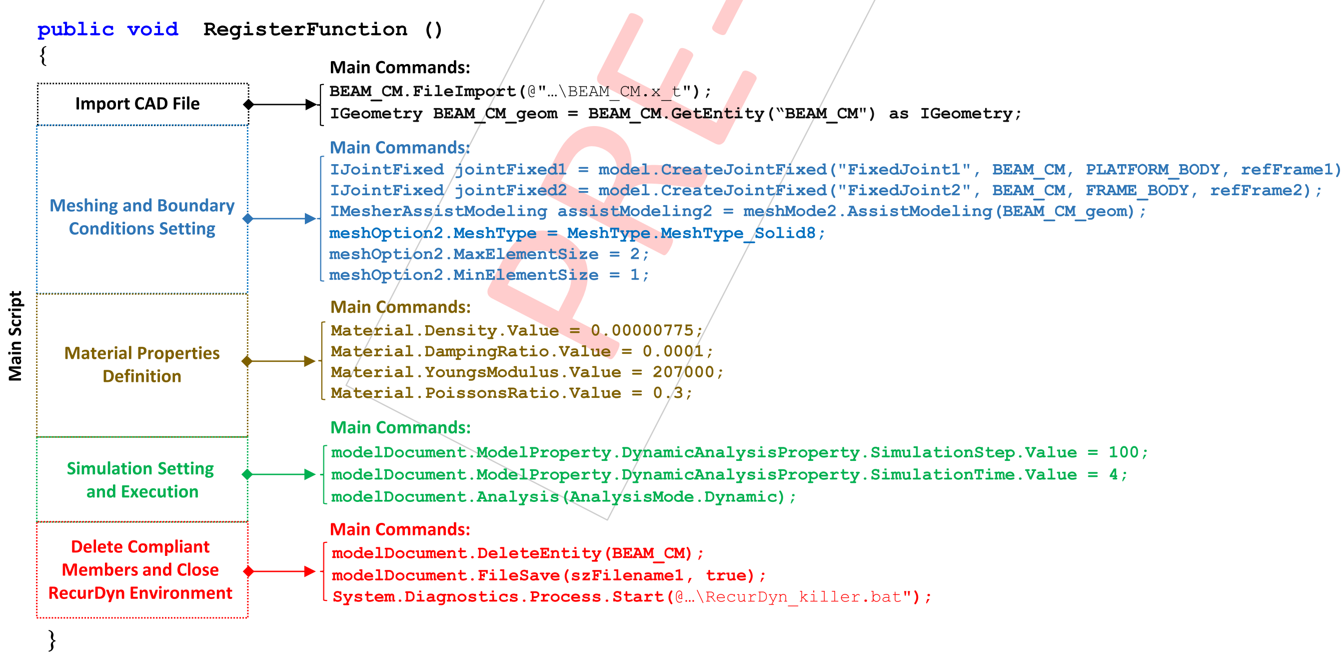

Fig. 6. ProcessNet script for optimization problem.

The complete optimization process, depicted in Fig. 7, has to be managed through a sequence of *Matlab* functions:

- **Creation of the Design Space & Definition of the Sampling Points** (similarly to Section 4.1);
- **For** K = 1 **to** Number of Sampling Points
  - **Update of the text file** connected with *PTC Creo* in order to modify the geometry of the compliant members;
  - **Batch*PTC Creo*Execution** to create the K-th Geometry of the compliant members;
  - **Batch*RecurDyn*Execution** of the K-th CM configuration. The model is managed by a *ProcessNet* Script (launched automatically from *RecurDyn*), that imports the K-th flexible model and enforces Joints, Mesh and Material Properties definition. Subsequently, the K-th simulation starts upon the execution of a *ProcessNet* command.
  - **Extraction** of the K-th results set and objective function evaluation (similarly to Section 4.1);

  end
- **Data fitting & Search of the minimum** (similarly to Section 4.1).

5. Validation of the method on a theoretical case

To validate the proposed optimization procedure, a simple theore-

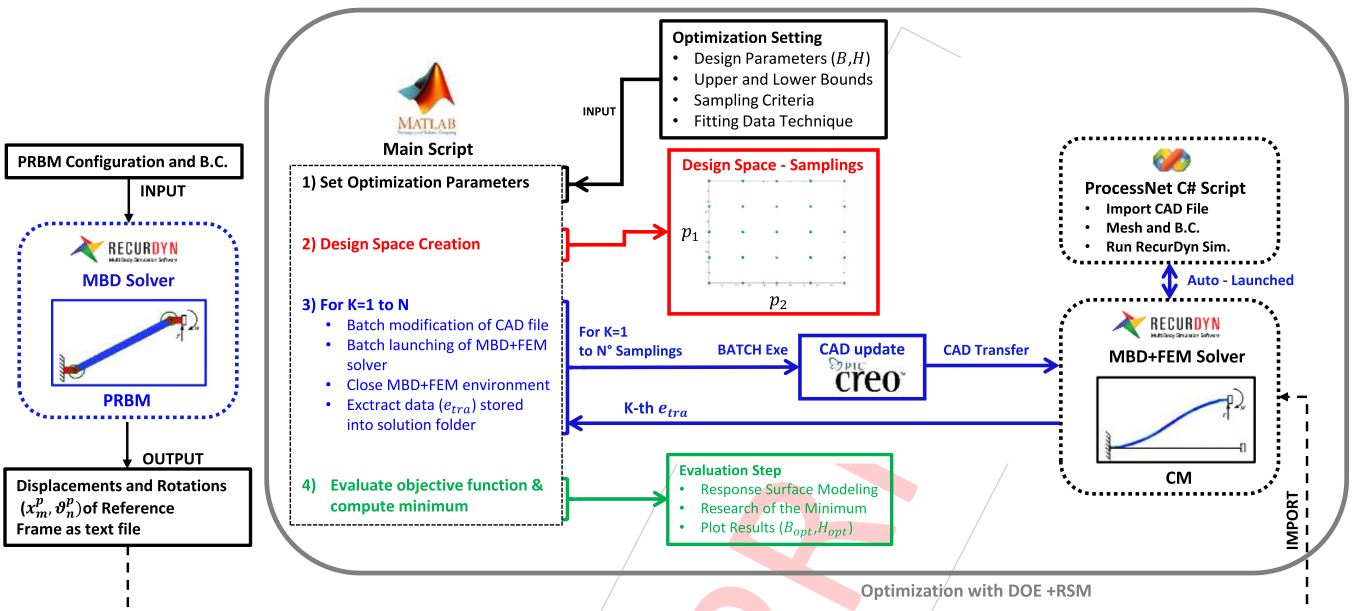

Fig. 7. Schematic of #Step 3 (CM shape optimization) loop.

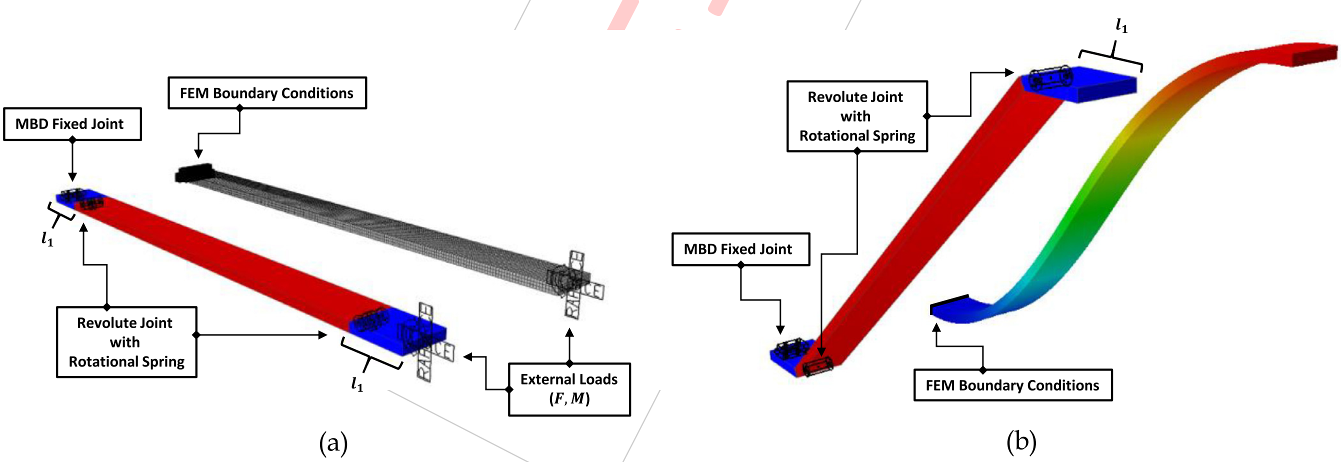

Fig. 8. Fixed-guided beam: MBD and nonlinear FEM. (a) Undeflected configuration; (b) Deflected configuration.

tical case study (shown in Fig. 8) with consolidated results is solved, namely a cantilever beam with rectangular section, as the one depicted in Fig. 3e. The beam length is l = 200mm, cross section's width and thickness are, respectively, B = 15mm and H = 3mm, Young's modulus, Poisson's ratio and yield strength of the employed material are, respectively, E = 0.4GPa, ν = 0.41, and σ_s = 30MPa.

The initial *RecurDyn* FEM model is obtained by a mapped mesh of brick elements (1 mm as max element size). After a mesh convergence analysis, the employed mesh consists of 9001 elements and 12865 nodes. For what concerns the loads acting on both flexible CM model and related PRB model, with reference to Fig. 8, a vertical upward force, F = 4.5N, and a clockwise moment, M = −336Nmm, are applied to the beam free end with a linearly growing law in a series of Q = 200 simulation steps, ensuring a maximum final deformation characterized by $\Theta_{\max}$ = 46. 6°, along with vertical and horizontal deflections respectively equaling a_c/l = 0.75and b_c/l = 0.59, and a maximum stress $\sigma_{\max}$ = 14.8MPa. Once the results from the nonlinear FEM are available, several parametric PRB models are tested, by leveraging on the framework described in Fig. 5. In particular, referring to this specific case study, the values for *characteristic radius factor* and *stiffness coefficient* suggested in the literature are, respectively, K_Θ = 2.68 and γ = 0.8517 [1]. The corresponding PRB links length and torsional stiffness can be obtained by means of Eqs. (6) and (11) as $l_1 = (1 - \gamma)l/2$ = 19.07mm and $K = 2\gamma K_\Theta EJ/l$ = 306.54Nmm/rad. These PRB parameters are computed considering the Euler-Bernoulli beam theory, whose limits are discussed in [5]. In parallel, the results achieved by means of the proposed software framework are summarized in Table 1. The same table also provides the values of the objective function $\hat{e}_{tra}$ from Eq. 23, highlighting that the approach proposed in this paper can provide better results than the analytical one.

Concerning the determination of the flexure geometry mimicking the PRB model (i.e. *#Step 3* in Fig. 2), the theoretical method described in Eq. (18) is compared with the results obtained employing the framework depicted in Fig. 7. The input of the problem are the PRB parameters, namely γ = 0.8517, τ = 4.57, a_p/l = 0.75 and K = 306.54 Nmm/rad, whereas the limit stress value is set to σ_{max} = 14.8 MPa (as computed in the initial FEM simulation). The results achieved by means of either the theoretical model or the software tool are summarized in Table 2, along with the corresponding *trajectory errors*.

Table 1
PRB derivation process: optimization results.

Pseudo-rigid-body parameters	*Analytical*	*Numerical*
γ	0.8517	0.8093
$\tau = 2\gamma K_\Theta$	4.57	4.55
Trajectory error ($\hat{e}_{tra}$)	0.042	0.009

Table 2
CM shape optimization results.

Compliant member cross section	*Analytical*	*Numerical*
B	15.78 mm	15.05 mm
H	2.94 mm	2.98 mm
Trajectory error ($\hat{e}_{tra}$)	0.015	0.010

Overall, the numerical results provided in Tables 1 and 2 confirm that the described procedure can be effectively employed for deriving reliable PRB parameters (i.e. *#Step 1* in Fig. 2) and for dimensioning the beam cross section (i.e. *#Step 3* in Fig. 2). Obviously, in this validation case, the results obtained during the shape optimization process, simply provide the values initially set for the flexure cross-section.

6. Validation of the method on a spatial compliant mechanism

6.1. #Step 1: PRB derivation process

In this section, a case study consisting of a spatial CM with flexures of complex geometry is analyzed. Let one first consider a particular linkage system, namely a spatial slider-crank mechanism (see Fig. 9), which transforms a rotational motion of an input crank into a purely translational motion of a slider (hereafter also referred to as platform). Such mechanism is composed of a revolute, two spherical and a prismatic pairs.

In order to reduce friction, the prismatic pair may be substituted by parallel leaf-spring flexures (i.e. a fully compliant four-bar linkage), which can provide approximate straight line guiding [27].

The initial CAD model of such partially compliant mechanism, along with its PRB counterpart, are depicted in Fig. 10. The flexible CM model is composed of three moving rigid bodies (crank, rod and platform), two rigid bodies fixed to the ground (motor and frame), and two flexible members (similarly to Fig. 1a) with constant cross section. With reference to Fig. 11, these flexures are initially designed as slender beams with length l = 400 mm, width B = 15 mm, and thickness H = 5 mm. The horizontal distance (in the x-direction) of the beams is set to d = 59 mm (also shown in Fig. 11). The length of crank and connecting rod are, respectively, 70 mm and 345 mm. It is evident that, due to the mechanism topology and the absence of a prismatic joint guiding the platform (as in Fig. 9), an out-of-plane motion of the platform itself may occur during functioning. This crucial aspect is highlighted in Fig. 10d, where the actual platform trajectory is shown, as compared to an ideal straight path achievable with the rigid-link mechanism shown in Fig. 9. For what concerns the CM of Figs. 10a and b, the compliant beams are made of Spring Steel with Young's Modulus, E = 207 GPa, and Poisson's ratio, ν = 0.30.

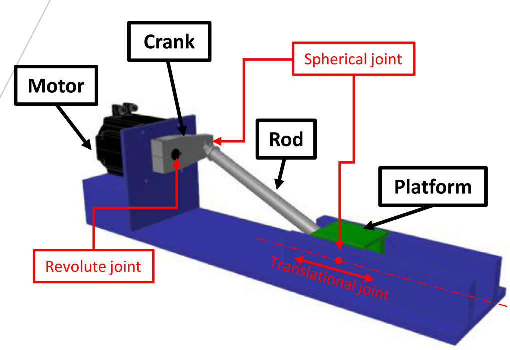

Fig. 9. Spatial Crank Mechanism.

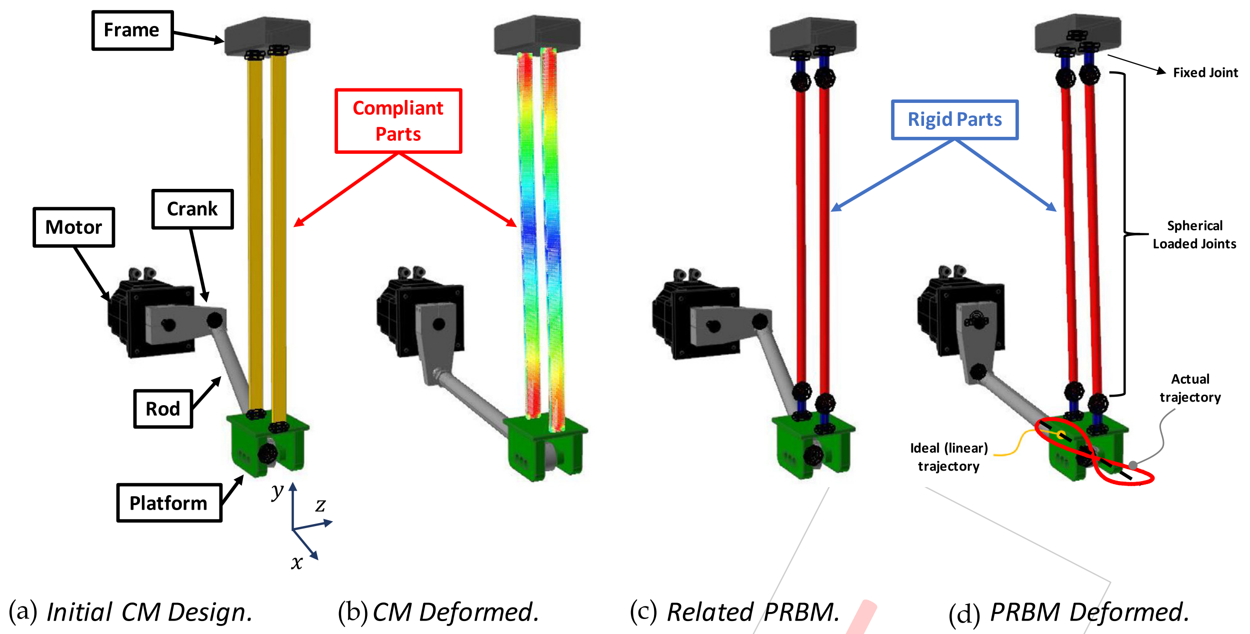

Fig. 10. Spatial Crank Mechanism connected to a fully compliant four-bar linkage.

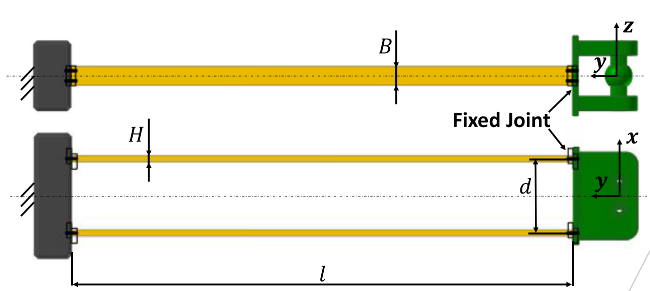

Fig. 11. Compliant four-bar linkage.

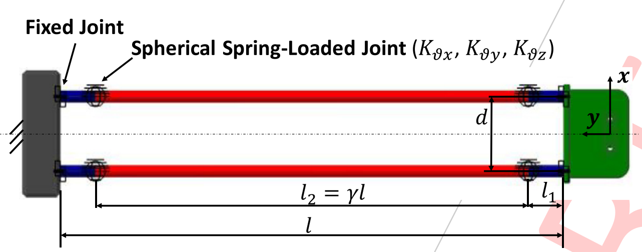

Fig. 12. Spatial four-bar linkage: PRB model.

Table 3
Optimization results for #Step 1.

PRB Parameters	γ	μ	ε	τ
	0.86	0.47	0.12	2.40
Trajectory error ($\hat{e}_{tra}$)	0.0007			

After a mesh convergence analysis, the employed mesh of this initial CM design consists of 4802 brick elements and 7238 nodes for each member. In order to allow the spatial motion of the platform, the PRB system (depicted in Fig. 10c) is formed by four equally-spaced S joints, each having a generalized rotational spring mounted in parallel. These four springs are characterized by the same rotational stiffness constants. Subsequently, with the purpose of measuring the *trajectory error*, e_{tra}, between CM and PRB systems, a reference frame is placed on a point of interest located on the platform (Figs. 11 and 12), while, in order to have a quasi-static behavior, a rotation at low constant velocity is enforced along the rotation axis of the crank (*0.25* rev/s). Owing to these assumptions, the PRB derivation process (*#Step 1* in Fig. 2) requires the determination of four design parameters, namely γ, μ, ε and τ, where γ is necessary for determining the length of each segment (see Fig. 12) and μ, ε and τ are directly related to the stiffness coefficients $K_{\vartheta x}$,$K_{\vartheta y}$, $K_{\vartheta z}$ of the spherical spring-loaded joints via Eq. (19), as previously discussed.

Numerical results concerning the PRB parameters determined by means of the framework described in Fig. 5 are summarized in Table 3, whereas Fig. 13a–c respectively report the behavior of CM and optimal PRB model in terms of spatial translations of the platform (along *x, y*, and *z* directions, shown in Fig. 10a). For all motion variables of the measured reference frame, the PRB model captures the CM behavior with excellent accuracy. In addition, Fig. 13d reports the rotation along the *x*-axis, highlighting the limits of the employed PRB topology, which is however considered sufficiently accurate for the proposed application. Rotations graphs along *y* and *x*-axis are extremely small (i.e. 0.01 rad of maximum values), thus they are not included for brevity.

6.2. *#Step 2: evaluation of design alternatives*

Considering the second phase of the conceptual design process shown in Fig. 2, by leveraging on the previously derived PRB model, *#Step 2* allows to quickly evaluate several design alternatives. In

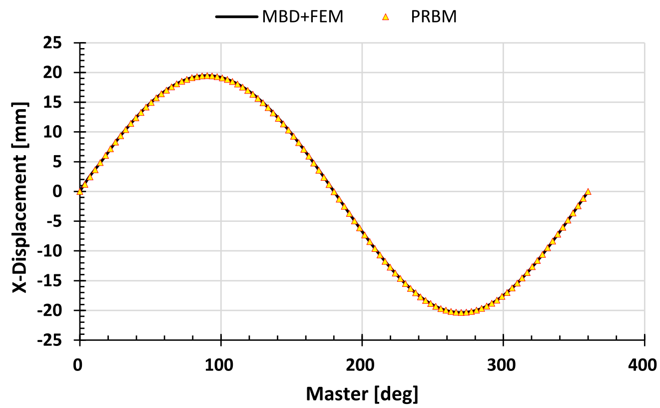

(a) *Displacement along the x-direction.*

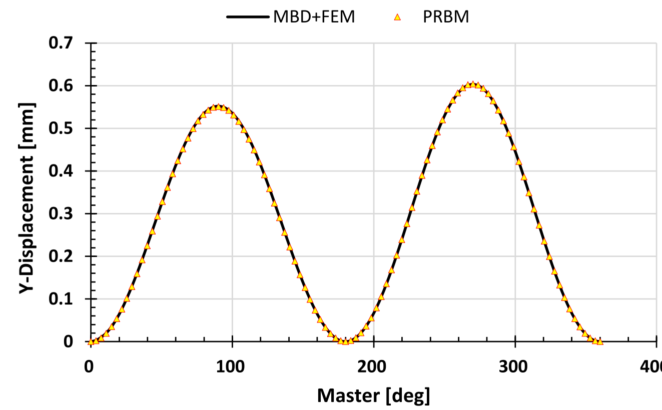

(b) *Displacement along the y-direction.*

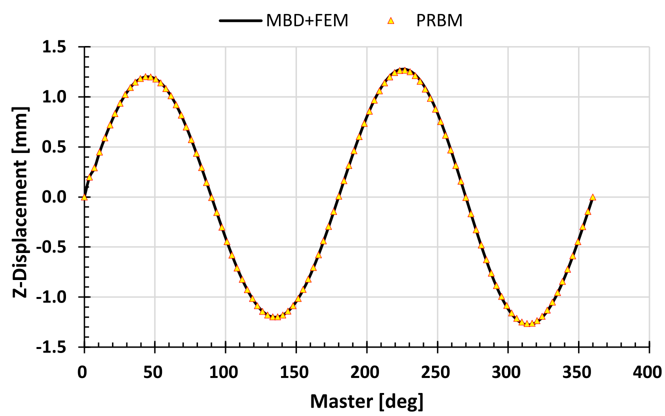

(c) *Displacement along the z-direction.*

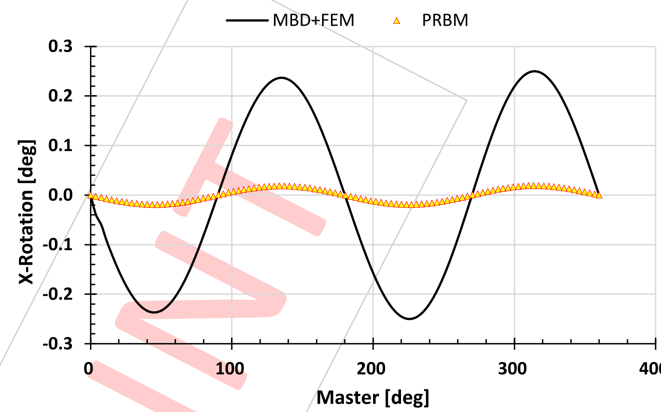

(d) *Rotation along the x-direction.*

Fig. 13. Comparison between flexible CM model and related PRB model: displacement plots.

particular, three measures of the mechanism performance, measured on its PRB implementation, will be evaluated hereafter, namely:

- Trajectory tracking of an ideal path;
- Required actuation torque measured on the motor shaft;
- Maximum bending stress arising in the flexures.

Regarding the first measure, since parallel leaf-spring flexures are employed to replace a prismatic joint acting on the platform (along x-direction), the kinematic performance of the PRB model may be evaluated by computing the actual platform trajectory and comparing it to a pure platform translation (ideal motion) that would be obtained by the rigid slider-crank mechanism. So the tracking error e_{lin}, between the platform's trajectory and the ideal profile (i.e. a straight line along the x-axis) can be defined as follows:

$$e_{lin}(K_{\vartheta x}(l, B, H), K_{\vartheta y}(l, B, H), K_{\vartheta x}(l, B, H), \ d), = e_{lin}(l, d, B, H) = \sqrt{\frac{1}{Q}\sum_{i=1}^{Q}\left[\sum_{j=1}^{2}|x_j^P - 0|\right]^2} \tag{24}$$

where x_1^P and x_2^P are, in this case, the displacements of the platform along y-direction and z-direction. As highlighted in Eq. (24), the trajectory tracking error is function of the flexure distance, d (see Fig. 11), along with the parameters $K_{\vartheta x}$, $K_{\vartheta y}$, $K_{\vartheta z}$. These latter stiffness values are, in turn, function of the flexure geometry via the parameters l and B (see Eq. (19)), which respectively represents flexure length and cross section's width. As for the actuation torque, it can be directly measured within the MBD environment, whereas the maximum bending stress (which is mainly function of the beam thickness, H [48]), is computed via Eq. (16). In particular, several DOE + RSM investigations have been performed considering $l \in [300, 350, 400, \ 450, 500]$ mm, $d \in [39, \ 49, \ 59, \ 69, \ 79]$mm, $B \in [10, \ 12, \ 15, \ 18, \ 25]$mm, and $H \in [3, 4, 5, 6, 7]$mm. The obtained results are reported in Fig. 14, that allows to easily evaluate a design solution that is suited to the functional requirements of the system in terms of the abovementioned quantities, i.e., trajectory tracking, maximum and RMS actuation torques, maximum stress. After the abovementioned investigation, the selected PRB model is characterized by a length $l = 500$ mm, a width $B = 18$ mm, a thickness $H = 4$ mm, and an unchanged distance $d = 59$ mm. Note that, as visible in Figs. 14a and b, the trajectory tracking performance reasonably increases as the flexures' length, l, and width, B, increase. However, in order to limit the maximum and RMS actuation torques, the beam width should not exceed a certain threshold (as visible in Figs. 14c and d). Regarding the maximum stress, the adopted flexure material (spring steel) provides a yield strength

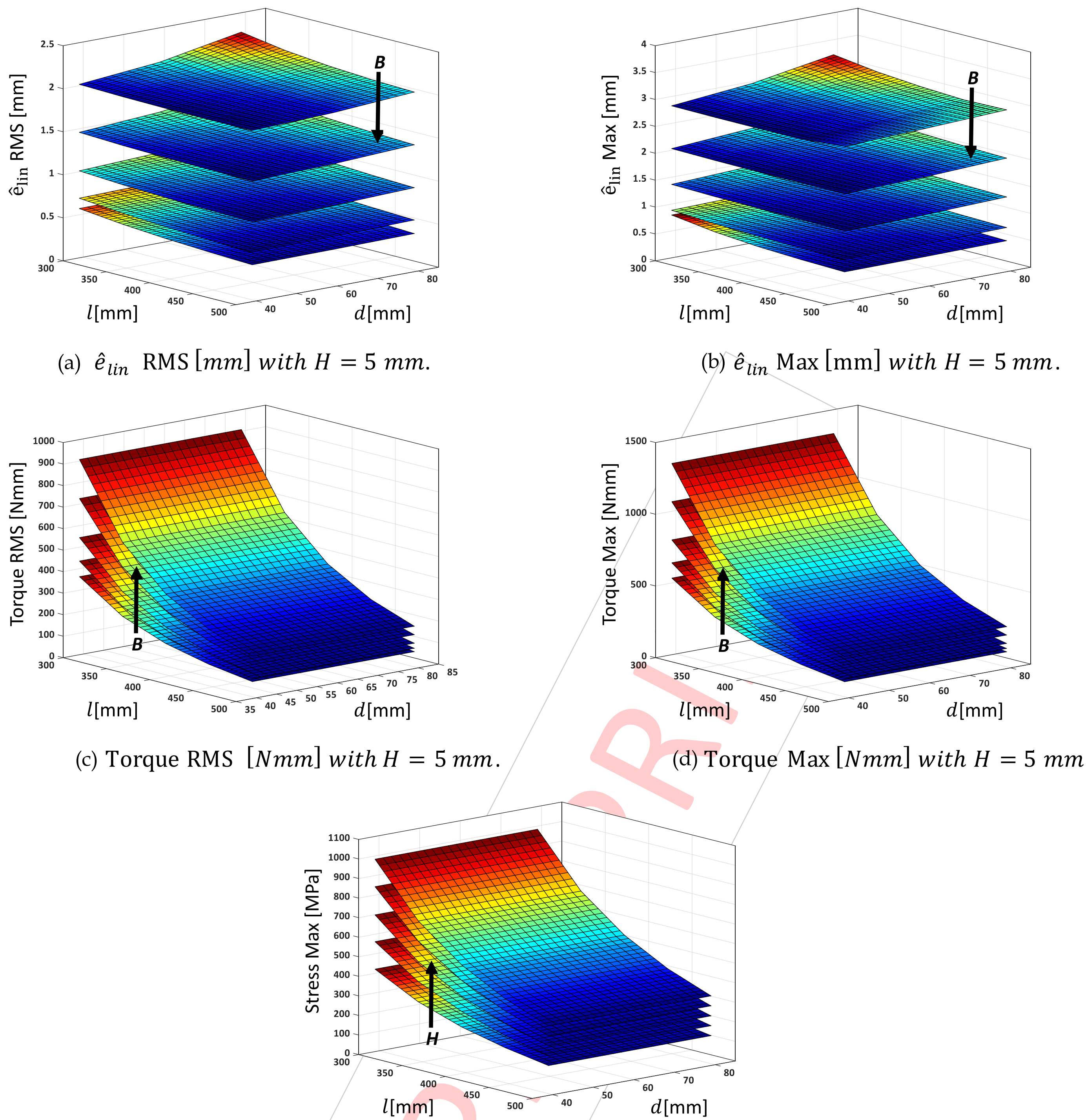

(a) $\hat{e}_{lin}$ RMS $[mm]$ $with\ H = 5\ mm.$ (b) $\hat{e}_{lin}$ Max [mm] $with\ H = 5\ mm.$

(c) Torque RMS $[Nmm]$ $with\ H = 5\ mm.$ (d) Torque Max $[Nmm]$ $with\ H = 5\ mm.$

(e) $Stress\ Max\ [MPa]\ with\ B = 20\ mm.$

Fig. 14. DOE + RSM investigation for the evaluation of design alternatives.

$\sigma_s = 1100$ MPa. Therefore, by adopting a flexure thickness $H = 4$ mm, the designer is enforcing a safety coefficient slightly higher than 2.

6.3. #Step 3: CM shape optimization

In order to obtain the final CM design, based on the PRB model evaluated in the previous section, the shape optimization scheme is employed and a hybrid flexure with non-standard shape is considered so as to demonstrate the generality of the proposed approach. In particular, hybrid flexures have been adopted in previous works [39] with the purpose of reducing the flexure stiffness in the direction of actuation, although the same design target could be achieved by simply decreasing the thickness of a simple beam or by employing materials with lower Young Modulus. In any case, it shall be remarked that the main purpose of the paper is to show that custom geometries with defined in-plane and out-of-plane stiffness characteristics and optimized according to complex design goals can be readily obtained via the proposed CAD/CAE framework. Specifically, let one consider numerical values obtained in #Sept 2 for the flexure distance, d (see Fig. 11) and for the PRB stiffness $K_{\vartheta x}$, $K_{\vartheta y}$, $K_{\vartheta x}$, which in turn define l, B

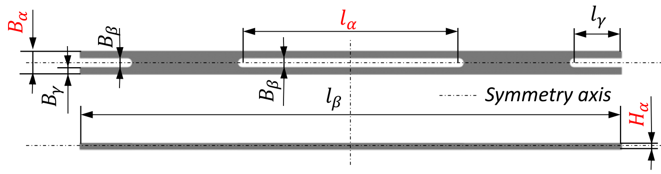

Fig. 15. Hybrid flexure of final CM design.

and H via Eq. (19) and a CM mechanism including hybrid flexure geometries, that comprise a number of eyelets, as shown in Fig. 15.

Let one then assume that:

- Two identical hybrid flexures shall be employed in place of the compliant parts shown in Fig. 11;
- With reference to Fig. 15 and Eq. (20), the chosen design parameters (among the many possible ones) defining the flexure geometric features are $p_1 = H_\alpha$, $p_2 = B_\alpha$, $p_3 = l_\alpha$
- With reference to Eq. (21), the following constraints are enforced:
  - $3.5\,\text{mm} \le p_1 \le 6\,\text{mm}$
  - $18.0\,\text{mm} \le p_2 \le 24.0\,\text{mm}$
  - $100.0\,\text{mm} \le p_3 \le 250.0\,\text{mm}$
  - $p_4 = l_\beta = 500\text{mm}$
  - $p_5 = l_\gamma = 45\text{mm}$
  - $p_6 = B_\beta = 7\ mm$
  - $p_7 = B_\gamma = B_\alpha - 2B_\beta$

As discussed before, in order to generate updated parametric geometries during design space exploration, the geometric model of the compliant members is parametrized in the *PTC Creo* environment. Since the CM is characterized by out-of-plane motions, the parameters chosen for the flexure geometry are directly related to its cross section's moments of inertia. The results of the shape optimization process are shown in Fig. 16a, where the function $\hat{e}_{tra}(p_1, p_2, p_3)$ and its minimum value are shown over the explored design space (by fixing $p_3 = 200$ mm for visualization purposes).

The optimal solution, that is $p_1 = H_\alpha = 4$ mm, $p_2 = B_\alpha = 19$ mm, $p_3 = l_\alpha = 200$ mm represents the final flexure geometry. In order to confirm the accuracy of the procedure, similarly to the *#Step 1*, a comparison between the optimized PRB model and the final CM is presented in Figs. 16b, c and d, which provide the position profiles of the two systems (PRB model and hybrid flexure CM) in the *x*, *y*, and *z* directions. Also, the path followed by the platform in the 3D space is provided in Fig. 17. As desired, the final CM design closely follows the behavior established by the PRB model, also confirming that the choice of the PRB topology is acceptable for the considered application. After the shape optimization routine, a final simulation test has been performed, in order to verify that the maximum Von Mises stress and the actuation torque at the motor shaft, that are, respectively, 580 MPa, 590 Nmm (maximum torque) and 397 Nmm (RMS torque). These values are compatible with the design constraints. For what concerns computational times, all the simulations have been performed on a Workstation with an Intel(R) Xeon(R) CPU E3-1270 v5 @ 3.6 GHz and

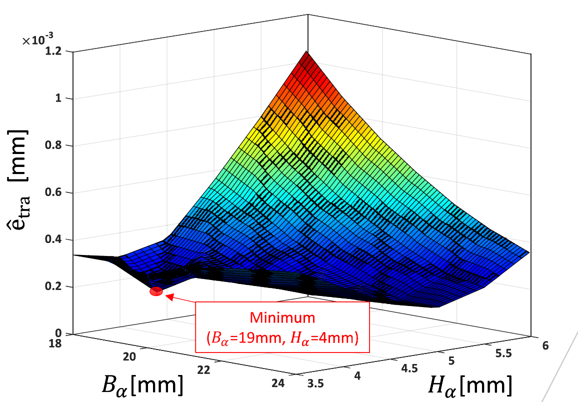

(a) *Optimal solution for $l_\alpha = 200mm$.*

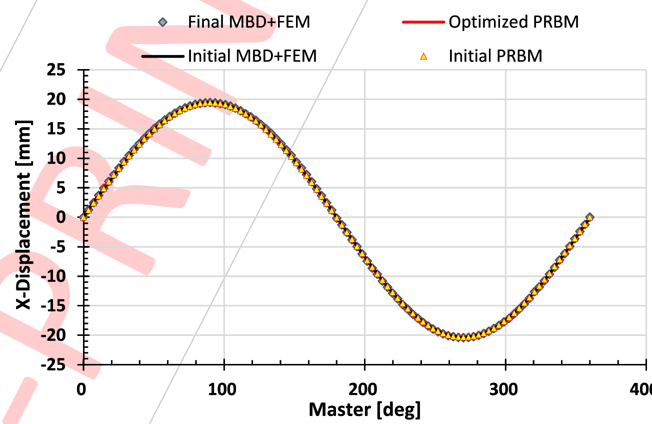

(b) *Displacement along the x-direction.*

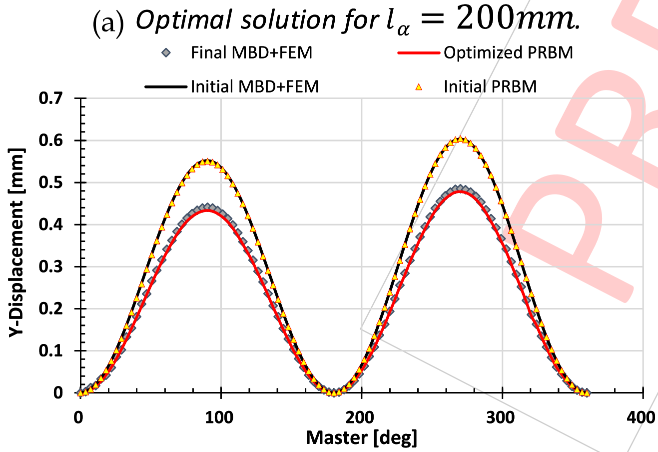

(c) *Displacement along the y-direction.*

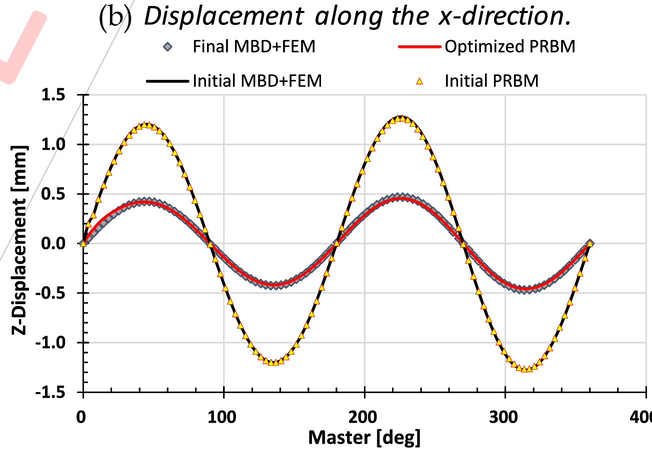

(d) *Displacement along the z-direction.*

Fig. 16. #Step 3 results: comparison between PRB model and CM behaviors and optimal solution.

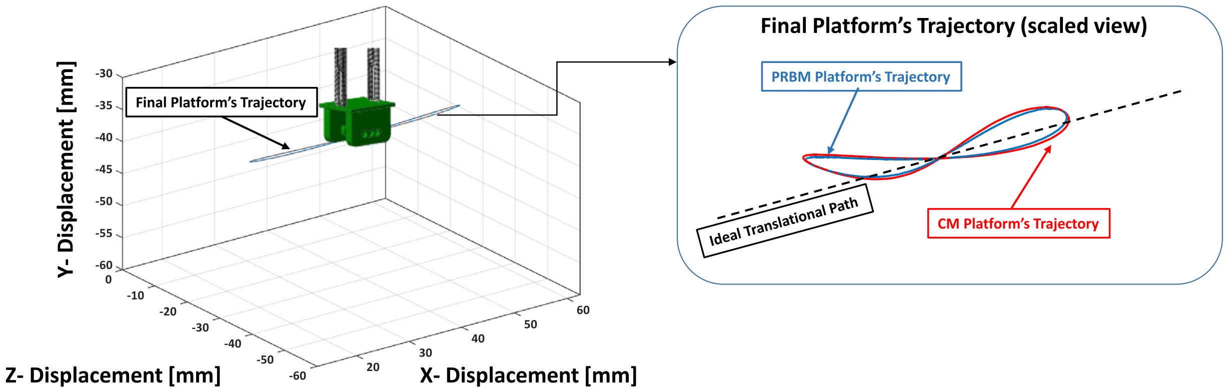

Fig. 17. 3D Platform's trajectory.

32 GB RAM. Every CM model is solved in *RecurDyn* in 200 s, whereas the PRB models are simulated in 0.37 s, further highlighting the usefulness of the PRB approximation whenever computational efficiency is sought after. Considering the framework defined for the *#Step 1* and *#Step 2* of the design process, a single iteration is computed in 3 s, due to the fact that *RecurDyn*'s is re-launched at each iteration. For what concern the *#Step 3*, every iteration is computed in about 220 s. In this case, the framework also embeds *PTC Creo* and a *ProcessNet* macro, thus increasing the total iteration time.

7. Conclusion

In this paper, a general engineering approach for designing spatial compliant mechanisms with hybrid flexures has been presented. The method leverages on the integration of a set of state-of-the-art CAE tools, namely *Matlab* (for meta-model based optimization), *RecurDyn* (for MBD/FEM simulation), and *PTC Creo* (for geometric modelling of complex shapes). This set of modelling tools allows for the determination of PRB models that replicate a given compliant mechanism topology, on one hand, and for the design of flexible members with complex geometry, on the other. After an initial validation of the proposed framework, carried out on a simple planar case study known from literature, the overall procedure has been tested on a spatial compliant mechanism with hybrid flexures. Numerical results confirm the suitability of the method for designing systems comprising a set of rigid and flexible bodies with non-standard customized geometry. Since the proposed approach is largely based on the use of general purpose CAD/CAE software, it shows good potentials for the quick and efficient design of optimized compliant systems in a large variety of applications.

Supplementary materials

Supplementary material associated with this article can be found, in the online version, at doi:10.1016/j.rcim.2018.07.015.

References

[1] L.L. Howell, Compliant Mechanisms, John Wiley & Sons, 2001.
[2] B. Zhu, Y. Lu, M. Liu, H. Li, X. Zhang, Fatigue study on the right circular flexure hinges for designing compliant mechanisms, ASME Int. Mech. Eng. Congr. Exposition (2017) Paper No. IMECE2017-70853, pp. V04AT05A012 (7).
[3] R. Bharanidaran, B.T. Ramesh, Design of compliant mechanism based microgripper with three finger using topology optimization, Int. J. Mech. Mechatron. Eng. 7 (7) (2013) 1385–1390.
[4] K.A. Tolman, E.G. Merriam, L.L. Howell, Compliant constant-force linear-motion mechanism, Mech. Mach. Theory 106 (2016) 68–79.
[5] Q. Meng, G. Berselli, R. Vertechy, V. Parenti Castelli, An improved method for designing flexure-based nonlinear springs, ASME IDETC/CIE, International Design Engineering Technical Conferences and Computers and Information in Engineering Conference, 4 2012, pp. 211–219.
[6] G. Palli, G. Berselli, C. Melchiorri, G. Vassura, Design of a variable stiffness actuator based on flexures, ASME J. Mech. Rob. 3 (3) (2011) 034501-034501-5.
[7] Ç.M. Tanık, V. Parlaktaş, E. Tanık, S. Kadıoğlu, Steel compliant cardan universal joint, Mech. Mach. Theory 92 (2015) 171–183.
[8] F. Parvari Rad, R. Vertechy, G. Berselli, V. Parenti-Castelli, Design and stiffness evaluation of a compliant joint with parallel architecture realizing an approximately spherical motion, Actuators 7 (20) (2018) 1–18.
[9] Q. Liang, D. Zhang, Z. Chi, Q. Song, Y. Ge, Y. Ge, Six-DOF micro-manipulator based on compliant parallel mechanism with integrated force sensor, Rob. Comput. Integr. Manuf. 27 (1) (2011) 124–134.
[10] Y. Yun, Y. Li, Optimal design of a 3-PUPU parallel robot with compliant hinges for micromanipulation in a cubic workspace, Rob. Comput. Integr. Manuf. 27 (6) (2011) 977–985.
[11] R. Crescenzi, M. Balucani, N.P. Belfiore, Operational characterization of CSFH MEMS technology based hinges, J. Micromech. Microeng. 28 (5) (2018) 055012(11).
[12] M. Verotti, A. Dochshanov, N.P. Belfiore, A Comprehensive Survey on Microgrippers Design: Mechanical Structure, ASME J. Mech. Des. 139 (6) (2017) 060801-060801-26.
[13] S. Awtar, A.H. Slocum, E. Sevincer, Characteristics of beam-based flexure modules, ASME. J. Mech. Des. 129 (6) (2006) 625–639.
[14] G. Berselli, A. Guerra, G. Vassura, A.O. Andrisano, An engineering method for comparing selectively compliant joints in robotic structures, IEEE/ASME Trans. Mechatron. 19 (6) (2014) 1882–1895.
[15] G. Hao, Creative Design and Modelling of Large-Range Translational Compliant Parallel Manipulators, Ph.D Thesis, Heriot-Watt University, School of Engineering and Physical Sciences, Edinburgh (2011).
[16] D.L. Blanding, Exact constraint: machine design using kinematic processing, ASME, N. Y. (1999).
[17] H. Su, H. Tari, On line screw systems and their application to flexure synthesis, ASME J. Mech. Rob. 3 (1) (2011) 011009-011009-7.
[18] J.B. Hopkins, M.L. Culpepper, Synthesis of multi-degree of freedom, parallel flexure system concepts via Freedom and Constraint Topology (FACT)-Part I: Principles, Precis. Eng. 34 (2) (2010) 259–270.
[19] J.B. Hopkins, M.L. Culpepper, Synthesis of multi-degree of freedom, parallel flexure system concepts via freedom and constraint topology (FACT)-Part II: Practice, Precis. Eng. 34 (2) (2010) 271–278.
[20] H. Li, G. Hao, R.C. Kavanagh, Position-space-based compliant mechanism reconfiguration approach and its application in the reduction of parasitic motion, ASME J. Mech. Des. 138 (9) (2016) 092301-092301-13.
[21] H. Li, G. Hao, Position-space-based design of a symmetric spatial translational compliant mechanism for micro-/nano-manipulation, Micromachines 9 (189) (2018) 1–18.
[22] G. Hao, H. Li, Conceptual designs of multi-degree of freedom compliant parallel manipulators composed of wire-beam based compliant mechanisms, Proc. Inst. Mech. Eng. Part C J. Mech. Eng. Sci. 229 (3) (2015) 538–555.
[23] C.J. Kim, Y.M. Moon, S. Kota, A building block approach to the conceptual synthesis of compliant mechanisms utilizing compliance and stiffness ellipsoids, ASME J. Mech. Des. 130 (2) (2008) 022308-022308-11.
[24] Q. Xia, T. Shi, Topology optimization of compliant mechanism and its support through a level set method, Comput. Meth. Appl. Mech. Eng. 305 (2016) 359–375.
[25] V. Venkiteswaran, O. Turkkan, H. Su, Speeding up topology optimization of compliant mechanisms with a pseudorigid-body model, ASME J. Mech. Rob. 9 (4) (2017) 041007-041007-9.
[26] G. Chen, X. Botao, H. Xinbo, Finding the optimal characteristic parameters for 3R pseudo-rigid-body model using an improved particle swarm optimizer, Precis. Eng. 35 (3) (2011) 505–511.
[27] D.M. Brouwer, J.P. Meijaard, J.B. Jonker, Large deflection stiffness analysis of parallel prismatic leaf-spring flexures, Precis. Eng. 37 (3) (2013) 505–521.
[28] X. Herpe, R. Walker, M. Dunnigan, X. Kong, On a simplified nonlinear analytical model for the characterization and design optimization of a compliant XY micro-motion stage, Rob. Comput. Integr. Manuf. 49 (2018) 66–76.
[29] F. Ma, G. Chen, Bi-BCM: A Closed-Form Solution for Fixed-Guided Beams in Compliant Mechanisms, ASME J. Mech. Rob. 9 (1) (2016) 014501-014501-8.
[30] H. Su, A pseudorigid-body 3R model for determining large deflection of cantilever beams subject to tip loads, ASME J. Mech. Rob. 1 (2) (2009) 1–9.
[31] K.K. Venkiteswaran, H. Su, A parameter optimization framework for determining

the pseudo-rigid-body model of cantilever-beams, Precis. Eng. 40 (2015) 46–54.
[32] B.D. Jensen, L.L. Howell, Identification of compliant pseudo-rigid-body mechanism configurations resulting in bistable behaviour, ASME J. Mech. Des. 125 (4) (2003) 701–708.
[33] A. Midha, L.L Howell, T.W. Norton, Limit positions of compliant mechanisms using the pseudo-rigid-body model concept, Mech. Mach. Theory 35 (1) (2000) 99–115.
[34] G. Berselli, M. Piccinini, G. Vassura, Comparative evaluation of the selective compliance in elastic joints for robotic structures, IEEE International Conference on Robotics and Automation, 2011, pp. 4626–4631.
[35] T.-F. Lu, D.C. Handley, Y.K. Yong, Position control of a 3 DOF compliant micromotion stage, ICARCV 2004 8th Control, Automation, Robotics and Vision Conference, 2 2004, pp. 1274–1278.
[36] N. Lobontiu, Compliant Mechanisms: Design of Flexure Hinges, CRC Press, 2002.
[37] G. Hao, X. Kong, R.L. Reuben, A nonlinear analysis of spatial compliant parallel modules: Multi-beam modules, Mech. Mach. Theory 46 (5) (2011) 680–706.
[38] D. Zhang, Z. Gao, Performance analysis and optimization of a five-degrees-of-freedom compliant hybrid parallel micromanipulator, Rob. Comput. Integr. Manuf. 34 (2015) 20–29.
[39] S. Satheeshbabu, G. Krishnan, Qualitative Mobility Analysis of Wire Flexure Systems Using Load Flow Visualization, ASME J Mech Rob. 8 (6) (2016).
[40] G. Hao, Simplified PRBMs of spatial compliant multi-beam modules for planar motion, Mech. Sci. 4 (2013) 311–318.
[41] I.A. Ramirez, C.P. Lusk, Spatial-Beam Large-Deflection Equations and Pseudo-Rigid-Body Model for Axisymmetric Cantilever Beams, ASME Int. Design Engineering Technical Conferences and Computers and Information in Engineering Conference, 6 2011, pp. 43–49.
[42] O.A. Turkkan, H. Su, DAS-2D: a concept design tool for compliant mechanisms, Mech. Sci. 7 (2) (2016) 135–148.
[43] J.B. Jonker, J.P. Meijaard, SPACAR-Computer program for dynamic analysis of flexible spatial mechanisms and manipulators, Multibody Systems Handbook (1990) 123–143.
[44] J. Wang, W. Niu, Y. Ma, L. Xue, H. Cun, Y. Nie, D. Zhang, A CAD/CAE-integrated structural design framework for machine tools, Int. J. Adv. Manuf. Technol. 91 (1-4) (2016) 545–568.
[45] E. Hardee, K. Chang, J. Tu, K.K Choi, I. Grindeanu, X. Yu, A CAD-based design parameterization for shape optimization of elastic solids, Adv. Eng. Software 30 (3) (1999) 185–199.
[46] G. Hao, H. Li, S. Kemalcan, G. Chen, J. Yu, Understanding coupled factors that affect the modelling accuracy of typical planar compliant mechanisms, Front. Mech. Eng. 11 (2) (2016) 129–134.
[47] F.M. Morsch, N. Tolou, J.L. Herder, Comparison of Methods for Large Deflection Analysis of a Cantilever Beam Under Free End Point Load Cases, ASME IDETC/CIE, International Design Engineering Technical Conferences and Computers and Information in Engineering Conference, 7 2009, pp. 183–191.
[48] S. Timoshenko, J. Goodier, Theory of Elasticity, McGrawHill, New York, 1951.
[49] M.S. Kim, D.O. Kang, S.J. Heo, Innovative design optimization strategy for the automotive industry, Int. J. Automot. Technol. 15 (2) (2014) 291–301.
[50] T.W. Simpson, J.D. Peplinski, P.N. Koch, J.K. Allen, Metamodels for computer-based engineering design: survey and recommendations, Eng. Comput. 17 (2001) 129–150.
[51] M. Cavazzuti, Optimization Methods: From Theory to Design, Springer, 2013.
[52] P. Bilancia, G. Berselli, L. Bruzzone, P. Fanghella, A Practical method for determining the pseudo-rigid-body parameters of spatial compliant mechanisms via CAE tools, Procedia Manuf. 11 (2017) 1709–1717.
[53] J.G. Wang, G.R. Liu, A point interpolation meshless method based on radial basis functions, Int. J. Numer. Methods Eng. 54 (2002) 1623–1648.